Z. Physik A 291, 53–70 (1979)

Zeitschrift
für Physik A

Alpha Decay Studies of Very Neutron Deficient Isotopes of Hf, Ta, W, and Re

S. Hofmann, W. Faust, G. Münzenberg, W. Reisdorf and P. Armbruster
Gesellschaft für Schwerionenforschung, Darmstadt, Germany

K. Güttner and H. Ewald
II. Physikalisches Institut, Universität Gießen, Gießen, Germany

Received November 27, 1978; Revised Version January 31, 1979

Very neutron deficient isotopes in the Hf-Re region were produced by bombarding targets of ^{107,109}Ag, ^{nat,108,110}Pd, and ^{103}Rh with ^{58}Ni accelerated by the linear accelerator UNILAC at GSI. After separation from the projectile beam by the velocity filter SHIP, the fusion products were implanted with their full recoil energy into a silicon surface barrier detector. The subsequent alpha decay of the implanted ions was measured with the same detector. In some of the experiments the evaporation residues were implanted into a position sensitive silicon surface barrier detector. With a newly developed position and time correlation technique parent daughter relationships, half lives, and α branching ratios of a large number of isotopes could be determined. In the investigated reactions the eleven new isotopes $^{161-164}$Re, ^{160}W, $^{157-161}$Ta, and ^{156}Hf could be identified. The measured Q_α values, half lives, and α branching ratios are discussed. Two new high energy α transitions of (7,408 ± 10) keV and (7,804 ± 15) keV were also found with half lives of 2.7 ms and 0.52 ms, respectively. A tentative mass and atomic number assignment gives $A = 153$–156 and $Z = 70$–72. The energies of the excited isomeric states are between 2 MeV and 3 MeV. From the systematics of alpha ground state transitions in even nuclei a hindrance of 10^5 can be deduced for both transitions, possibly indicating orbital angular momenta on the order of $10\hbar$ for the alpha emitting states. The isomers are proposed to belong to shell model isomers beyond ^{146}Gd.

1. Introduction

The establishment of complete alpha decay systematics throughout the chart of nuclei is a long standing goal in nuclear physics. Alpha decay studies are a valuable tool of nuclear spectroscopy [1]. In recent years nuclei that are increasingly further removed from the valley of stability have been the object of investigations. Specifically, for neutron numbers between the $N = 82$ and $N = 126$ neutron shells, the most recent publications have been concerned with Ytterbium isotopes with mass numbers 153–158 ($N = 83$–88) and their alpha daughters [2] and with Rhenium ($A = 166$–169), Osmium ($A = 165$–168), and Iridium ($A = 168$–170) isotopes [3–5]. The former investigation has shown that ^{153}Yb ($N = 83$) is not an alpha emitter as expected from the predicted drop by about 2 MeV of the Q_α value when crossing the 82 neutron shell. No alpha emitters with $N = 83$ or 82 have been found to this date.

Despite these and a number of older studies [6], there is still a large number of nuclear species, predicted to be stable or quasistable against proton radioactive decay, that are missing from the systematics. To our knowledge no alpha emitting Ta isotopes are known in the literature. Four Re isotopes $^{166-169}$Re have been claimed only very recently [3, 4].

Our knowledge to date of accurate partial half lives for alpha decay in this range of the chart of nuclei is even more incomplete.

Another new dimension has been added to spectroscopic studies of nuclei just above the $N = 82$ neutron shell by the discovery of an island of high spin isomers [7]. These studies used primarily gamma spectroscopic tools. It seems reasonable to expect that some of these high spin isomers may have a measurable width for alpha decay. The relative sim-

0340-2193/79/0291/0053/$03.60

plicity of alpha spectroscopy could then be a valuable complementation to the more complex γ ray studies in both identifying these states and giving clues to their structure.

The work presented here has been started at GSI with the aim to obtain comprehensive alpha spectroscopic data for proton rich isotopes between the $N=82$ and $N=126$ neutron shells. Among the methods used to produce very proton rich nuclei, two have been particularly successful in the past. Spallation reactions induced by 600 MeV proton beams have been used at the Isolde Facility [8]. The lack of selectivity of this reaction mechanism which allows to produce copious amounts of many different nuclear species is overcome by the use of on-line electromagnetic isotope separators.

The second method has been using heavy ion (HI) induced fusion reactions together with gas jet techniques. Helium jets have the advantage of combining high efficiency with reasonably fast separation times. For moderately proton rich nuclei the new isotopes are generally identified as (HI, xn) evaporation residues and the reaction mechanism is fairly selective. This identification technique becomes increasingly more ambiguous, however, as the proton drip line is approached. Very proton rich excited compound nuclei produced in fusion reactions deexcite by a multitude of evaporation paths due to the increased significance of charged particle emission. Even at relatively moderate excitation energies of (30–40) MeV, typical for $3n$ reactions, one observes with comparable or higher cross sections $2np$, $n2p$, $3p$, αnp, $n2\alpha$, etc. products. The excitation functions of all these evaporation products due to the emission of 3 particles are very similar.

A further difficulty which becomes apparent close to the proton drip line and which limits both gas jet and isotope separator techniques is the rapid drop in half lives below the 100 ms level.

In this work we have used very heavy proton rich ions as ^{58}Ni available at the UNILAC accelerator together with an electromagnetic velocity filter [9] to overcome some of the above difficulties.

The velocity filter efficiently separates projectiles from fusion products in times sufficiently short, typically 1 μs, to allow the investigation of very short lived species. The choice of ions as heavy as ^{58}Ni together with proton rich targets allows to make weakly excited compound nuclei by fusion that are very close to the region of interest near the proton drip line. It will be shown that in many cases the problem of unambiguous identification of alpha lines can be overcome by implanting the fusion products that have passed the velocity filter directly into position sensitive solid state detectors. This allows to use position and time correlation methods that make a rather efficient use of parent daughter relationship for isotope identification as well as alpha branching ratio determination.

In the course of this work eleven new isotopes could be identified and a number of alpha branching ratios were measured. The fast separation has also allowed us to find two new high energy alpha lines that are very likely due to high spin isomeric transitions. Preliminary results have been given elsewhere [10, 11]. In Sect. 2 we describe the experimental method. Detailed results grouped into four alpha decay families, each starting with a new Re isotope ($^{161-164}$Re), are presented in Sect. 3. A discussion of the new extended Q_α systematics, partial alpha half lives, and reduced α widths together with an estimate of the character of the new high energy transitions will be given in Sect. 4.

2. Experimental Method

Targets of Rh, Pd, and Ag isotopes were irradiated with a beam of ^{58}Ni ions accelerated by the UNILAC at GSI to search for decay properties of new isotopes in the region from Hafnium to Rhenium. With an average beam current of $2 \cdot 10^{10}$ ions/s typical collecting times were on the order of 10 min. Target properties, as well as projectile beam energies, and compound nucleus excitation energies are summarized in Table 1.

Table 1. Properties of the irradiated targets, energies of ^{58}Ni projectiles, and excitation energies of the compound nuclei calculated with mass values from Takahashi et al. [41]

Target			$E_{Proj.}$ [MeV]	Compound nucleus	Excitation energy [MeV[a]]
Isotope	Enrichment resp. purity [%]	Thickness [(μg/cm^2)]			
^{109}A	99.4	1,160	263	^{167}Re	44–57
			275		52–65
^{107}Ag	99.5	1,230	263	^{165}Re	39–52
		130	263		51–52
		1,230	275		47–60
		130	275		59–60
^{110}Pd	97.7	1,090	215	^{168}W	23–36
			263		56–68
^{108}Pd	98.9	980	215	^{166}W	20–31
			263		52–63
^{nat}Pd	99.5	1,180	263	W	43–56
			275		51–64
^{103}Rh	99.5	1,320	215	^{161}Ta	13–28
			263		44–59
			275		53–67

[a] Values are calculated for reactions at the end and at the beginning of the targets

After separation from the projectile beam in a velocity filter the reaction products are directly implanted into a solid state detector. In the following subsections we briefly describe the velocity filter SHIP (Sect. 2.1), the implantation method (Sect. 2.2), and a newly developed position time correlation method for isotope identification and determination of half lives as well as alpha branching ratios (Sect. 2.3).

2.1. The Velocity Filter SHIP

The principle of the separation of fusion products from the projectile beam with the velocity filter SHIP [9] is shown in Fig. 1. A combination of two electric and four magnetic dipole fields together with two quadrupole triplets accepts radially and axially an angular range of $\pm 1.5°$ relative to the projectile beam axis and focusses ionic charges within a charge window of $\pm 10\%$ onto a measuring position 11 m downstream of the target position. The velocity dispersion necessary to separate projectiles and evaporation residues is largest in the median plane of the ion optical system. Here a variable velocity slit allows to select a maximum velocity window of $\pm 5\%$. The velocity dispersion in the median plane is compensated in the second, symmetric, half of the instrument. Two thin carbon foils of about 30 $\mu g/cm^2$, 3 cm behind the target and in front of the velocity slit are used for ion charge equilibration of the fusion products and of background projectiles, respectively.
The special transmission properties of the velocity filter result in optimal target thicknesses of about 1 mg/cm^2. Calculated total efficiencies [12] for reactions with ^{58}Ni projectiles range from about 20% for xn and pxn channels to about 3.5% for αxn channels. The velocity filter is therefore partially selective for xn and pxn fusion products. The excellent

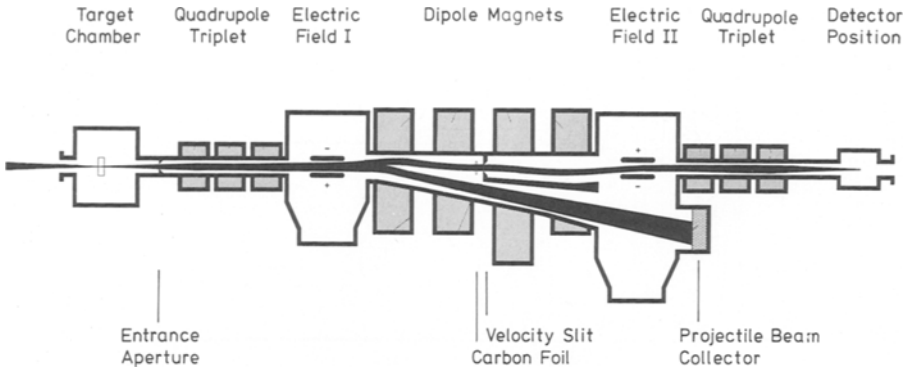

Fig. 1. Separation of evaporation residues from projectiles by the velocity filter SHIP

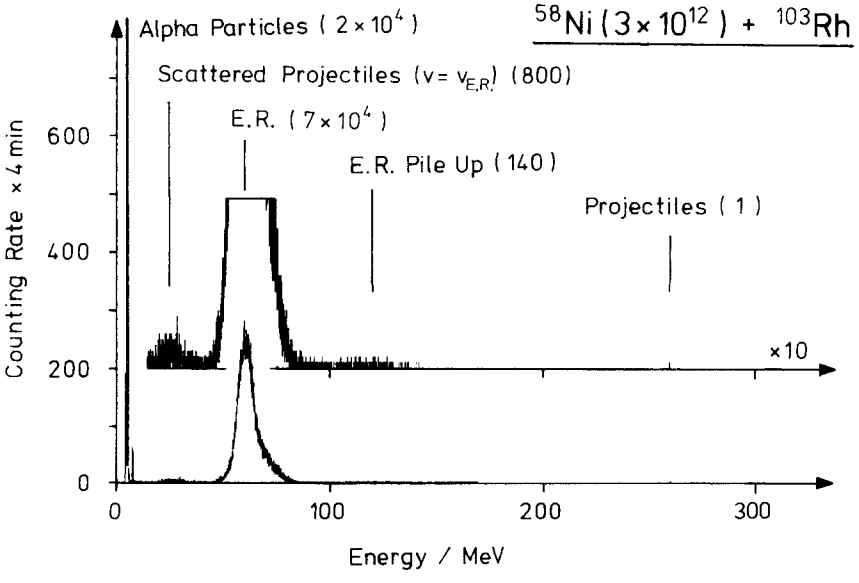

Fig. 2. Energy spectrum of implanted evaporation residues of the reaction ^{58}Ni (276 MeV) + $^{103}Rh \rightarrow {}^{161}Ta^*$. The number of collected particles is given in parenthesis

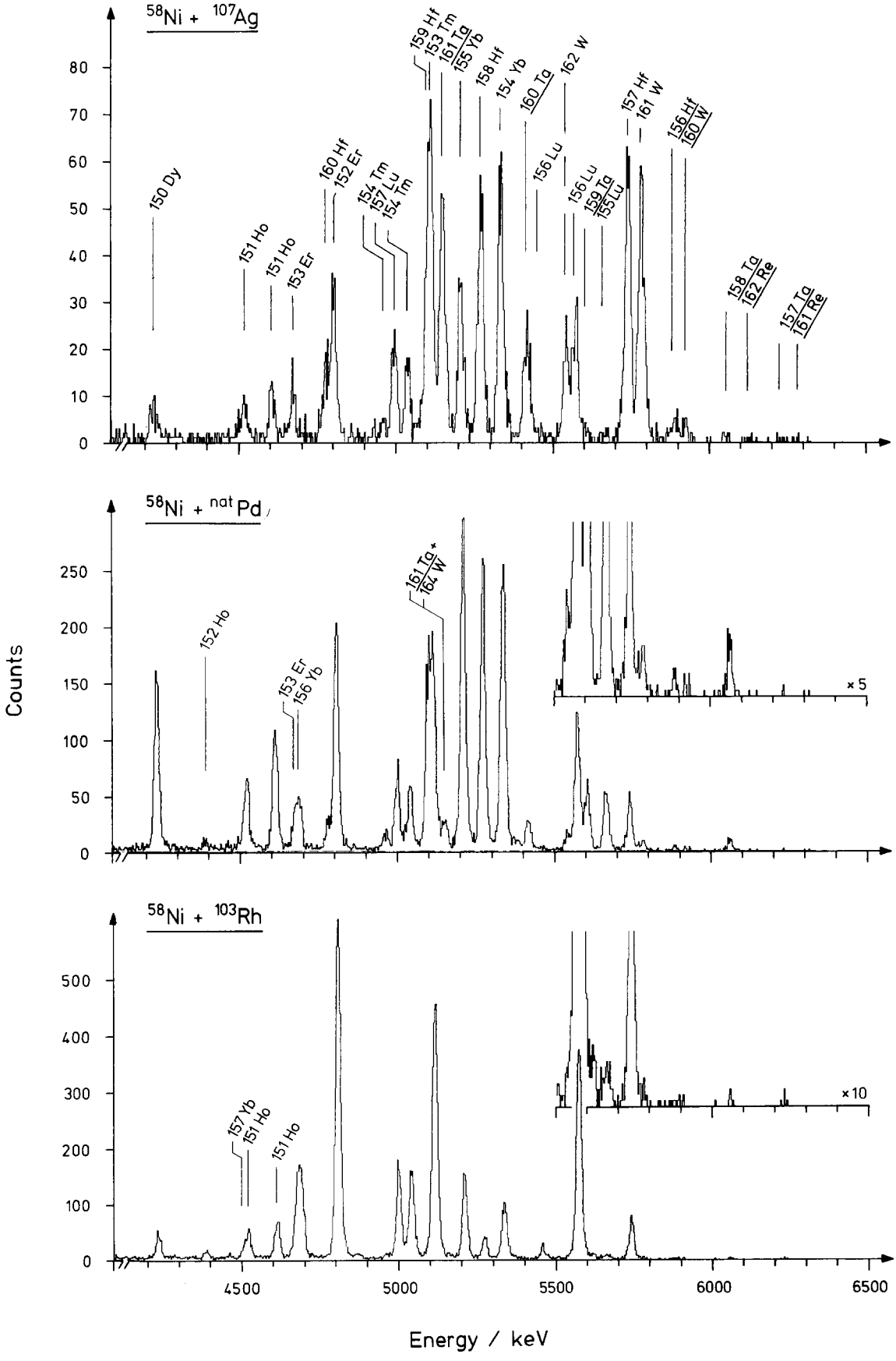

Fig. 3. α singles spectra of implanted evaporation residues taken during the irradiation of ^{107}Ag, ^{nat}Pd, and ^{103}Rh targets with 276 MeV ^{58}Ni projectiles. All α lines could be identified. Underligned are the new isotopes

selectivity from the projectile beam is illustrated in Fig. 2 which shows a typical energy spectrum obtained with a silicon surface barrier detector (450 $mm^2 \times 300$ μm) in the measuring position behind the velocity filter. Out of 3×10^{12} projectiles only one was registered by the detector at the primary beam energy. The peak at 60 MeV corresponds to evaporation residues. The energy distribution of ^{58}Ni ions that are scattered into the velocity window of the instrument is seen to peak near 25 MeV.

2.2. *The Implantation Method*

The sharp peaks at the lower end of the spectrum in Fig. 2 are due to α particles from the decay of the implanted evaporation residues. The implantation depth of the fusion products with average incident energies of 60 MeV into the detector material can be estimated to be about 7 μm [13]. From a comparison with the ranges of typical α particles one can estimate that an average of 65% of the α decays of the implanted fusion products are registered with full energy. The remaining fraction of α particles leaves the detector depositing a variable energy down to about 1.5 MeV.

The generally present small background of scattered ^{58}Ni ions was completely eliminated in the spectra by gating between UNILAC macropulses. The macroperiod of the accelerator is 20 ms with a beam pulse width of about 4 ms. The complexity of the alpha spectra obtained in various reactions is illustrated in Fig. 3.

With a 300 mm^2 surface barrier detector, cooled down to −15 °C it was possible to achieve a resolution of 17 keV at FWHM. We conclude that the implantation method combines the advantages of high geometrical efficiency with excellent resolution.

The implantation method requires special care with the energy calibration, since the detector also registers the recoiling daughter nuclei. Typical recoil energies are 150 keV, roughly half of which is converted into electron hole pairs giving rise to increased alpha signals as compared to signals from external alpha sources. The calibration was therefore made internally using six known alpha emitters identified in the on-line spectra. The corresponding energies are tagged with the superscript *b* in Table 2, column 2. This method assumes that the registered recoil energy is proportional to the alpha energy. A linear least squares fit to the six known alpha energies resulted in standard deviations of less than 5 keV.

2.3. *Isotope Identification, Half Life, and Alpha Branching Ratio Determination: A new Position and Time Correlation Method*

Unambiguous identification of new alpha lines is best performed in establishing decay chains leading to known transitions. A technique of position and time correlation measurements between subsequent decay signals was developped. The evaporation residues were implanted into a position sensitive silicon surface barrier detector with a width of 47 mm and a height of 8 mm. The width of the fusion product beam at the detector position behind the velocity filter was about 25 mm. Energy, time, and position of implantation of the incident evaporation residues and of the emitted alpha particles were measured. A typical alpha spectrum obtained with the position sensitive detector is shown in Fig. 4a.

The position resolution of the solid state detector was 400 μm (FWHM). This is large compared to the range, 7 μm at 60 MeV [13], of the implanted fusion products, their very small estimated recoil path, 0.4 μm, after alpha emission, and typical ranges of the alpha particles themselves, (25–40) μm. The main point of the method described here is that for any incident nucleus, its subsequent chain of alpha decays must be observed at its position of implantation within the limits of the resolution of the detector. This is illustrated in Fig. 4b for the parent daughter pair ^{161}W – ^{157}Hf. For each signal from an alpha particle emitted with an energy corresponding to the ^{161}W alpha transition the relative position signal from the subsequent daughter decay was registered, giving the position correlation spectrum shown.

The rate of random position correlations is strongly reduced by introducing a maximum limit for the time interval between signals to be correlated. The smallest meaningful time window is given by the half lives to be expected for the decays. To keep the random rate low, this time window must be small compared to the average rate of incidence and decay of the fusion products within the narrow position bands of about 1 mm defined by the finite detector resolution. Figure 4d shows a time correlation spectrum for the pair ^{161}W – ^{157}Hf. The origin of the time axis is defined by an observed ^{161}W decay, the points represent the number of observed subsequent ^{157}Hf decays. The decreasing rate reflects the half life of the daughter which can be determined from the spectrum by an exponential fit. One can see from the figure that the rate of random events, which should contribute to a flat background, was small. The half life of the parent nucleus can be obtained by studying the time correlation with the incident fusion products.

It immediately follows from the above observations

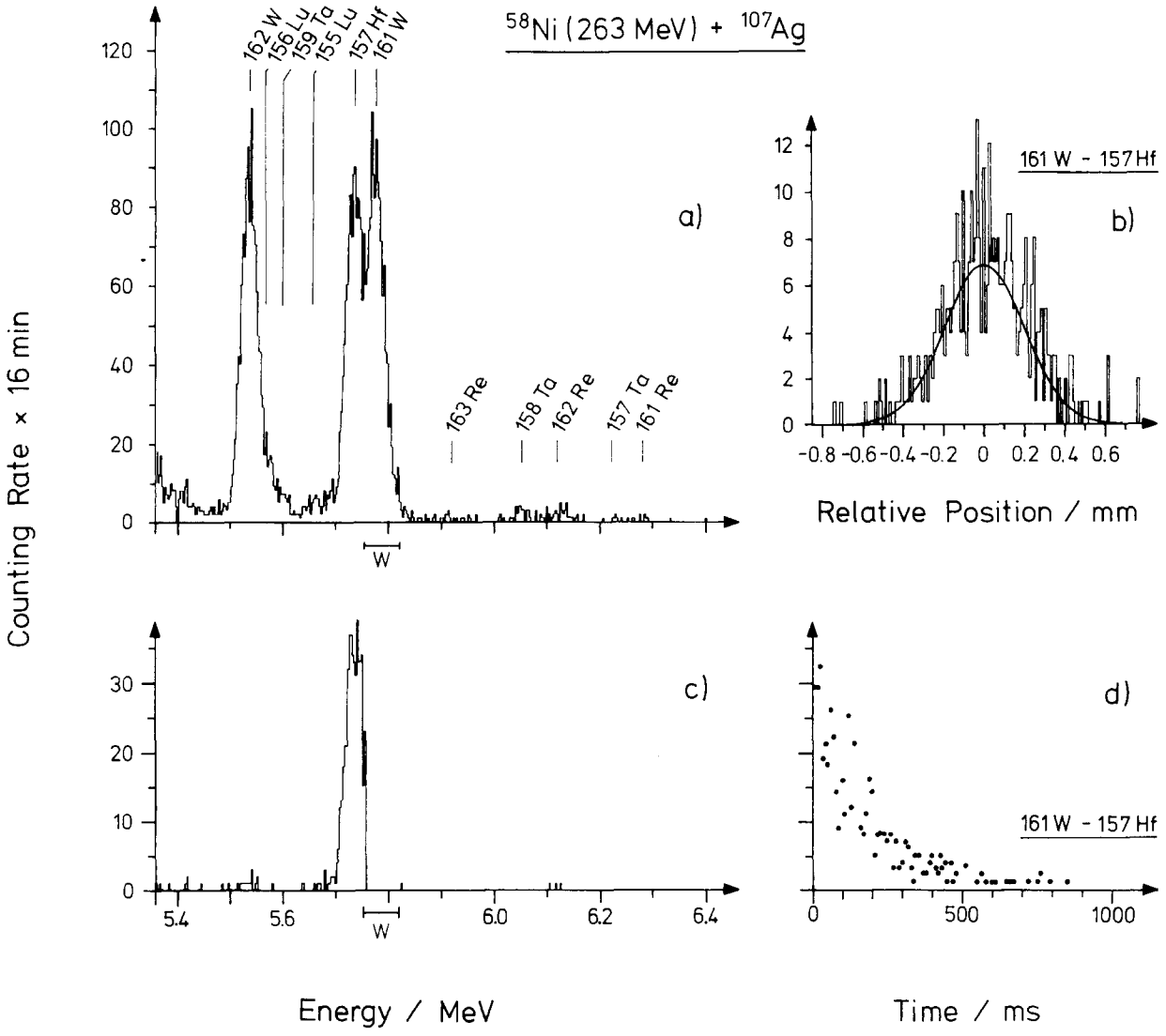

Fig. 4a–d. α singles spectrum of evaporation residues implanted into a position sensitive silicon surface barrier detector **a**; position distribution of α particles from the daughter ^{157}Hf relative to the position of α particles from the parent ^{161}W **b**; α spectrum correlated to the α line in the energy window *W*, Fig. 4a, gated in position, Fig. 4b, and time, Fig. 4d, **c**; time spectrum of the α lines from the decay ^{161}W $-^{157}$Hf **d**

that the correlation method makes it possible to measure alpha branching ratios with good precision. Corrections have to be made for loss of events by particle emission into the backward hemisphere (Sect. 2.2).

The parent daughter correlation, already established by the sharp position correlation peak in Fig. 4b and by the time correlation spectrum in Fig. 4d, is impressively confirmed by the completely isolated daughter alpha peak in Fig. 4c obtained from the spectrum in Fig. 4a by putting an energy window on the parent alpha line, as indicated, and by using a relative position window of ±0.5 mm and a relative time window of 900 ms.

Due to high countrates it was not always possible to measure half lives with the correlation method. In these cases we pulsed the UNILAC beam with a chopper, to obtain the decay characteristics.

3. Results

In the course of this work 36 isotopes were identified. Eleven of these are new isotopes. They are shown in the extract of the chart of nuclei, Fig. 5. For 2 of the 25 previously known isotopes the half life or the alpha energy was found to be significantly different from values reported in the literature. In many cases uncertainties in the values could be reduced. A sum-

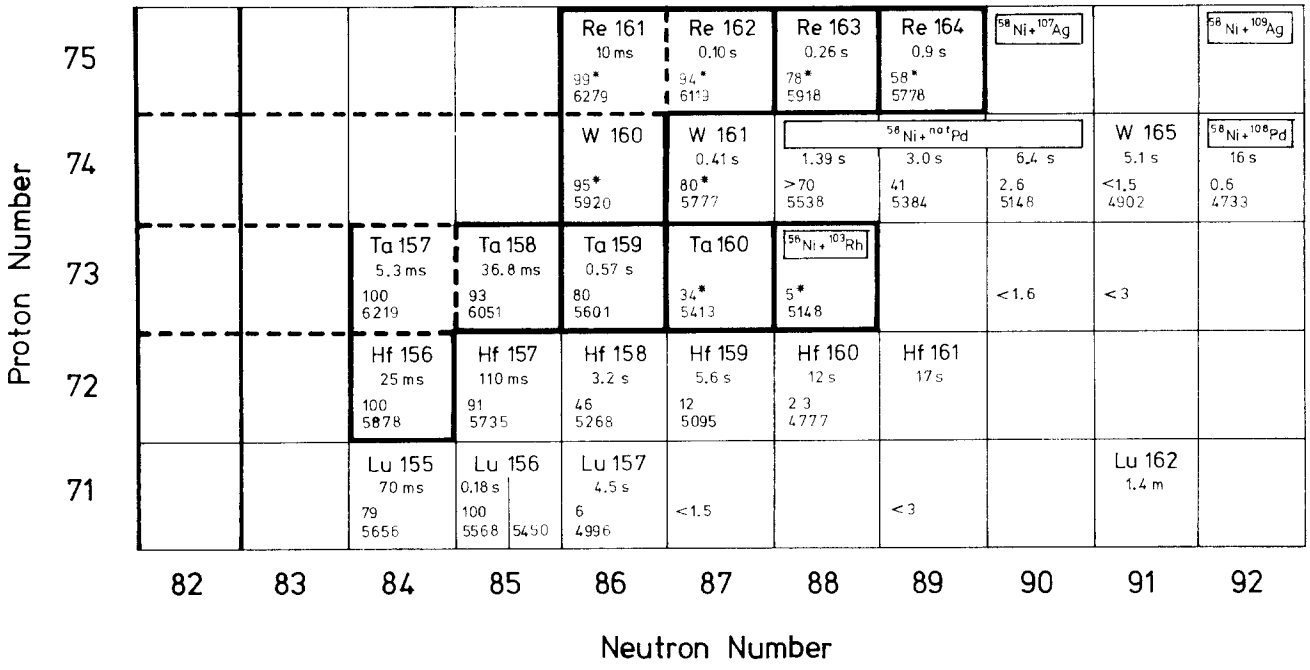

Fig. 5. Section of the chart of nuclei showing the neutron deficient isotopes of the elements between Lu and Re. Marked are the compound nuclei formed in the investigated reactions and the new isotopes. For all known isotopes the atomic numbers and half lives are given. Alpha energies, in keV, and α branching ratios, in per cent, are given for isotopes which were identified in the present work. Calculated α branchings are marked by an asterisk. The dashed line is the proton drip line calculated with the mass values of Myers [24]

mary of all identified isotopes with the measured alpha energies, half lives, and alpha branching ratios is given in Table 2.

In the following sections it is helpful to note that all the nuclides discussed in this work fit into four decay chain families (Fig. 6a–d) with one of the new isotopes ^{161,162,163,164}Re as the heaviest element isotope. The figures indicate measured α and deduced β branches. We will discuss the various nuclides in terms of these four decay chains.

3.1. *The Decay Chain of* ^{162}*Re* (Fig. 6a)

We have assigned ^{162}Re and ^{158}Ta to a pair of alpha peaks at (6,119 ± 6) keV and (6,051 ± 6) keV, respectively. Both were observed in the reaction ^{58}Ni + ^{107}Ag → ^{165}Re, E^* = (50–60) MeV. The correlation analysis showed unambiguously that both lines had a parent daughter relationship. The higher energy line was assigned to a Re isotope on the basis that it was not seen in reactions leading to tungsten compound nuclei. The mass assignment was possible from excitation function considerations using the observed production of the unambiguously identified isotope ^{163}Re as basis, see Sect. 3.3 and Fig. 7. It was not possible to follow this part of the decay chain beyond ^{158}Ta, because ^{154}Lu, its alpha daughter, probably has a very weak alpha branch due to its low Q_α value, and ^{158}Hf, the β daughter, is fed very strongly through a different mechanism: the alpha decay of ^{162}W as will be seen later. The half life of ^{162}Re, (100 ± 30) ms, was measured with the chopper method, the half life of the daughter ^{158}Ta, (36.8 ± 1.6) ms, was determined with the correlation method, which also gave the alpha branching of (93 ± 6)% for ^{158}Ta. For ^{162}Re an alpha branching of 94% has been estimated from calculated alpha and beta half lives, Sect. 4.2.

Alpha peaks from the decay chain starting with ^{162}W were prominent in all the reactions studied here. The observed alpha energies along the main decay path

$$^{162}\mathrm{W} \xrightarrow{\alpha} {}^{158}\mathrm{Hf} \xrightarrow{\alpha} {}^{154}\mathrm{Yb} \xrightarrow{\alpha} {}^{150}\mathrm{Er} \xrightarrow{\beta+}$$

$$^{150}\mathrm{Ho} \xrightarrow{\beta+} {}^{150}\mathrm{Dy} \xrightarrow{\alpha} {}^{146}\mathrm{Gd}$$

agree well with previously measured values. The half life of ^{162}W was measured with the chopper method resulting in the value of (1.39 ± 0.04) s. This is in disagreement with the earlier value of Eastham and Grant [19], who reported an upper limit of 0.25 s. The alpha branching ratio of ^{162}W is larger than 70%. This limit was obtained from the alpha in-

Table 2. Summary of α decay measurements and comparison with calculated α and β partial half lives

Isotope	E_α/keV	$T_{1/2}$ exp.	b_α/% exp.[f]	b_α/% calc.[f]	$T_{1/2,\alpha}$ exp.	$T_{1/2,\alpha}$ calc.	$T_{1/2,\beta}$ exp.	$T_{1/2,\beta}$ theor. [37]
^{164}Re[a]	5,778±10	(0.9 ±0.7) s		58		1.3 s		1.8 s
^{163}Re[a]	5,918± 6	(260 ±40) ms	>6	78		360 ms		1.3 s
^{162}Re[a]	6,119± 6	(100 ±30) ms	>3	94		61 ms		1.0 s
^{161}Re[a]	6,279±10	(10^{+15}_{-5}) ms	>1	99		16 ms		1.1 s
^{166}W	4,733±10[c]	(16 ±3) s[e]	0.6± 0.2	0.05	(2.7 ±1.0) ks	44 ks	(16 ±3) s	20 s
^{165}W	4,902±20[c]	(5.1 ±0.5) s[e]	<1.5	0.15	>300 s	5.4 ks	(5.2 ±0.5) s	8 s
^{164}W	5,148± 5[b]	(6.4 ±0.8) s[c]	2.6± 1.7	2.5	(230 ±150) s	310 s	(6.2 ±0.5) s	8 s
^{163}W	5,384± 5[b]	(3.0 ±0.2) s[c]	41 ± 5[c]	14	(7.3 ±1.0) s	24 s	(5.1 ±0.5) s	4 s
^{162}W	5,538± 5[c]	(1,390±40) ms[d]	>70[c]	44	(2.0 to 1.4) s	5.0 s	<4.6 s	4 s
^{161}W	5,777± 5[c]	(410 ±40) ms		80		490 ms		2 s
^{160}W[a]	5,920±10			95		140 ms		2.5 s
^{161}Ta[a]	5,148± 5			5		100 s		5.5 s
^{160}Ta[a]	5,413± 5			34		6.2 s		3.2 s
^{159}Ta[a]	5,601± 6	(570 ±180) ms	80 ± 5	77	(710 ±230) ms	970 ms	(2.8 ±1.1) s	3.2 s
^{158}Ta[a]	6,051± 6	(36.8 ±1.6) ms	93 ± 6	99	(40 ±3) ms	16 ms	$(0.5^{+3.3}_{-0.25})$ s	2.3 s
^{157}Ta[a]	6,219±10	(5.3 ±1.8) ms	100 ±23	100	(5.3 ±2.0) ms	3.9 ms	>15 ms	1.3 s
^{160}Hf	4,777± 5[c]	12 s[e]	2.3± 0.6[c]	0.5	(520 ±140) s	2.6 ks	12.3 s	13 s
^{159}Hf	5,095± 5[e]	(5.6 ±0.5) s[e]	12 ± 1[c]	11	(47 ±6) s	62 s	(6.4 ±0.6) s	8 s
^{158}Hf	5,268± 5[b]	(3.2 ±0.6) s[c]	46 ± 3	39	(6.1 ±0.6) s	9.8 s	(5.2 ±0.5) s	6.2 s
^{157}Hf	5,735± 5[d]	(110 ±6) ms[c]	91 ± 7	98	(120 ±10) ms	96 ms	$(1.2^{+4.6}_{-0.5})$ s	5 s
^{156}Hf[a]	5,878±10	(25 ±4) ms	100 ±19	99	(25^{+6}_{-4}) ms	27 ms	>0.1 s	3.2 s
^{157}Lu	4,996± 5[c]	(4.5 ±1.5) s[e]	6 ± 2	14	(75 ±35) s	62 s	(4.8 ±1.6) s	10 s
^{156}Lu	5,450±10[c]	~0.5 s[e]		95		0.51 s		8 s
^{156}Lu	5,568± 5[c]	(180 ±20) ms[c]	100 ±25	98	(180^{+50}_{-20}) ms	160 ms	>0.6 s	8 s
^{155}Lu	5,656± 6[c]	(70 ±6) ms[c]	79 ± 4	99	(89 ±9) ms	73 ms	(0.33 ±0.07) s	6.2 s
^{158}Yb	4,069±10[c]	(99 ±12) s[e]	<0.9	0.003	>9.7 ks	3.3 Ms	(99 ±12) s	100 s
^{157}Yb	4,505±10[c]	(38.6 ±1.0) s[e]		0.4		7.4 ks		32 s
^{156}Yb	4,686±10[c]	(24 ±1) s[e]	21 ± 6	4	(110 ±33) s	750 s	(30 ±3) s	32 s
^{155}Yb	5,206± 5[c]	(1.59 ±0.22) s[c]	84 ±10	90	(2.0 ±0.3) s	2.1 s	(10 ±6) s	18 s
^{154}Yb	5,332± 5[c]	(410 ±30) ms[c]	93 ± 2	97	(450 ±23) ms	580 ms	(6 ±2) s	20 s
^{154}Tm	4,959± 5[c]	(5 ±1) s[e]	44 ±15	72	(11 ±8) s	9.6 s	(9 ±5) s	25 s
^{154}Tm	5,035± 5[c]	(3.5 ±0.1) s[e]		86		4.1 s		25 s
^{153}Tm	5,109± 5[c]	(1.58 ±0.15) s[e]	95^{+5}_{-8}[c]	94	(1.7 ±0.2) s	1.9 s	$(32^{+\infty}_{-21})$ s	32 s
^{153}Er	4,674±10[c]	(36 ±1) s[c]	53 ± 3[e]	56	(68 ±4) s	80 s	(77 ±5) s	100 s
^{152}Er	4,802± 5[b]	(9.8 ±0.3) s[e]	93 ± 4[c]	86	(10.5±0.6) s	18 s	(140 ±80) s	110 s
^{151}Ho	4,519± 5[c]	(35.6 ±0.4) s[e]	18 ± 5[e]	56	(198 ±55) s	160 s	(43 ±3) s	200 s
^{151}Ho	4,606± 5[b]	(47 ±2) s[e]	13 ± 4[e]	78	(362 ±112) s	55 s	(54 ±3) s	200 s
^{151}Dy	4,068±10[c]	(1,080±12) s[e]	5.9± 0.6[e]	5	(18.3±1.9) ks	19 ks	(1,148±15) s	1.0 ks
^{150}Dy	4,232± 5[b]	(430.2±1.2) s[e]	38 ± 5[c]	34	(1.10±0.15) ks	1.9 ks	(694 ±56) s	1.0 ks
^{149}Tb	3,963±10[c]	(14.6 ±0.3) ks[e]	16 ± 4[e]	5	(91 ±23) ks	24 ks	(17.4 ±0.9) ks	1.3 ks

[a] New isotope; all newly measured values in columns 2, 3, and 4 are given without index

[b] The following literature values were used for energy calibration: ^{150}Dy: (4,233±4) keV [14]; ^{151}Ho: (4,607±3) keV [15]; ^{152}Er: (4,799 ±3) keV [15]; ^{158}Hf: (5,270±10) keV [18]; ^{163}W: (5,385±5) keV [19]; ^{164}W: (5,150±5) keV, mean value of Ref. [19] and Ref. [20]

[c] Value agrees with literature [2, 3, 6]; errors could be reduced in many cases

[d] Value differs significantly from literature [6]

[e] Literature value [2, 6, 15]; not measured in present work

[f] $b_{\alpha,\mathrm{exp}} = I_{\alpha,\mathrm{daughter}}/I_{\alpha,\mathrm{parent}}$ from α intensity ratios, $b_{\alpha,\mathrm{theor}} = T_\beta/(T_\alpha + T_\beta)$ from theoretical α and β half lives

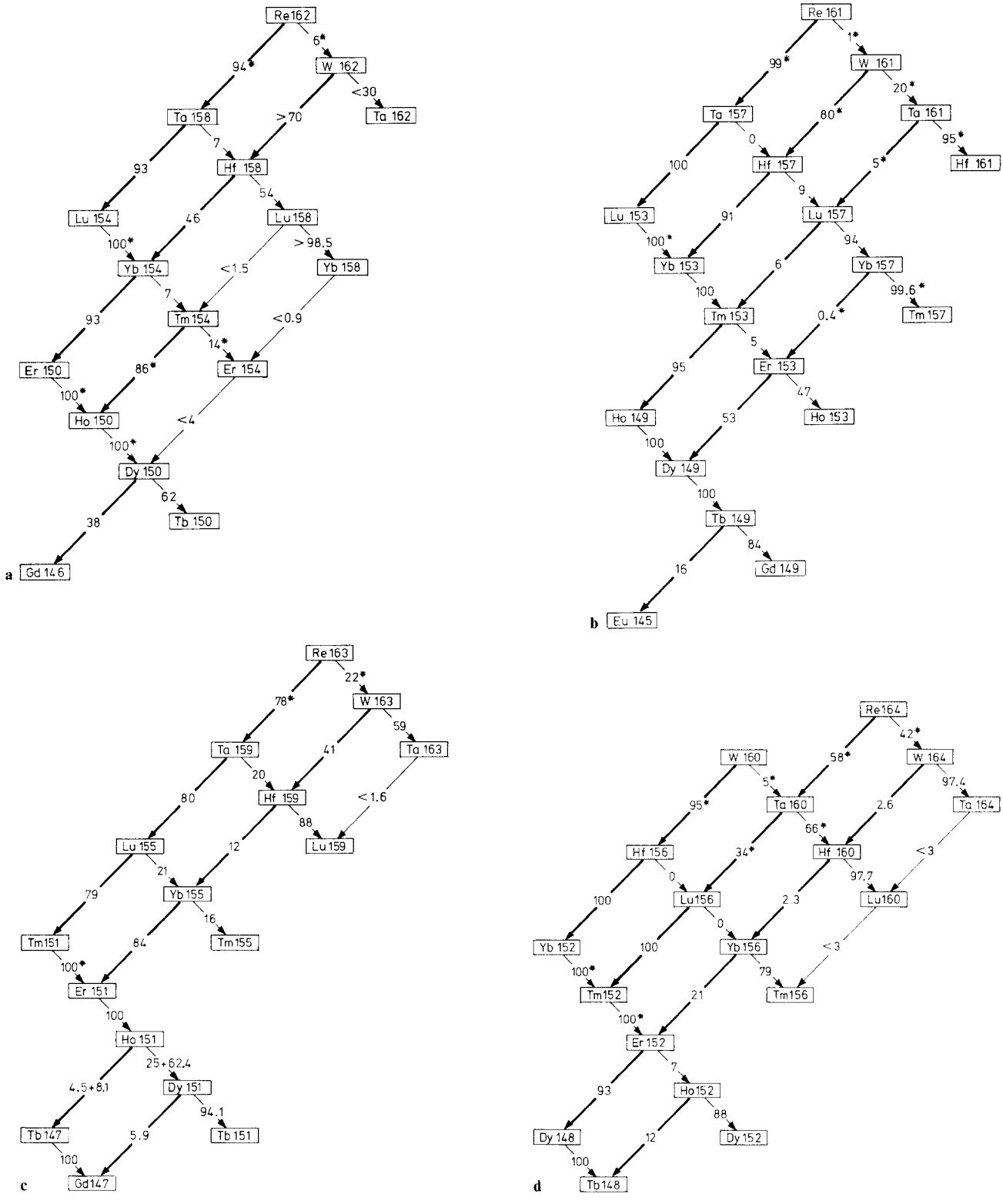

Fig. 6. a Decay chain of ^{162}Re with α and β branchings for each isotope in per cent. Calculated branchings are marked with an asterisk. Boldface arrows represent measured α transitions. **b** Decay chain of ^{161}Re. **c** Decay chain of ^{163}Re. **d** Decay chain of ^{164}Re

tensity ratio $^{166}Os/^{162}W$ observed in the reaction $^{84}Kr+^{93}Nb \rightarrow ^{177}Ir$ [5].

The half life of ^{158}Hf was measured by time correlation with its parent ^{162}W. The value of (3.2 $\pm$0.6) s is in agreement with earlier results [19, 22]. The alpha branching ratio of ^{158}Hf is found to be (46 $\pm$3)% from the ratio of mother and daughter intensities.

Similarly, by time correlation, a half life of (410 $\pm$30) ms was determined for ^{154}Yb. It is in very good agreement with literature values [2, 22]. The intensity ratio of the ^{158}Hf and ^{154}Yb alpha lines gives an alpha branching ratio of (93$\pm$2)% for ^{154}Yb.

From the measured alpha branching ratio for ^{158}Hf it follows that ^{158}Hf decays into ^{158}Lu with a probability of (54$\pm$3)%. A possible alpha line from ^{158}Lu should have an energy of about 4.8 MeV from systematic arguments. No alpha line around this energy was found in spectra with a high ^{158}Hf peak, giving an upper limit of 1.5% for the alpha branching ratio of ^{158}Lu.

The isotope ^{154}Tm is fed from the (7$\pm$2)% ε decay branch of ^{154}Yb. Two ^{154}Tm alpha lines are known in the literature [22]. Whenever direct production of ^{154}Tm could be expected to be unlikely, only the lower energy peak at 4,959 keV was observed. It was therefore assumed that the decay of ^{154}Yb feeds only the lower state in ^{154}Tm and an alpha branching ratio of (44$\pm$15)% was deduced for this state. No alpha branching ratio could be determined for the higher energy state in ^{154}Tm corresponding to an observed alpha transition energy of 5,035 keV. This state has an estimated alpha branching of 86%.

Hagberg et al. [2] found recently in a mass separated sample an alpha emitter at 4,069 keV which was assigned to ^{158}Yb. A 4,068 keV line seen here is assigned to ^{151}Dy [6] rather than ^{158}Yb. In the reaction $^{58}Ni+^{107}Ag \rightarrow ^{165}Re$ ($E^*=46$ MeV) we observed 10^4 counts in the ^{158}Hf alpha line. The competitive ε decay of similar intensity should feed ^{158}Yb via two subsequent decays. We deduce an upper limit of 0.9% for the alpha branching ratio of ^{158}Yb.

The ^{154}Er alpha line at 4.15 MeV, observed by Macfarlane and Griffioen [23] was not seen here. ^{154}Er should be populated mainly from decay of either of the two states in ^{154}Tm. We deduce an upper limit of 4% for the alpha decay branch of ^{154}Er.

For ^{150}Dy an alpha branching ratio of (38$\pm$5)% was obtained, in excellent agreement with the value of (36 $\pm$5)% in Ref. 2. In calculating this branching ratio it was assumed that ^{150}Dy is mainly populated from the decay of ^{154}Yb and ^{154}Tm and that ^{150}Er and ^{150}Ho are pure β emitters with half lives short compared to the 7.2 m half life of 150 Dy.

3.2. The Decay Chain of ^{161}Re (Fig. 6b)

The parent daughter pair $^{161}Re-^{157}Ta$ was identified with the same method and similar arguments as the pair $^{162}Re-^{158}Ta$ discussed in Sect. 3.1. We will therefore state here only the results: The alpha energy, half life, and alpha branching ratio of ^{157}Ta were found, respectively, to be (6,219$\pm$10) keV, (5.3 $\pm$1.8) ms and 100% (>77%). The α energy for ^{161}Re is (6,279$\pm$10) keV, its half life, which could be obtained by observing its decay characteristic during the 15 ms beam macro-pause, is $\left(10^{+15}_{-5}\right)$ ms. Estimates of the alpha branching for ^{161}Re run close to 100%.

Alpha peaks from ^{161}W and its daughters were most prominent in the reaction $^{58}Ni+^{107}Ag \rightarrow ^{165}Re$ ($E^*=52$ MeV). Eastham and Grant [20] have reported the observation of an alpha decay branch of ^{161}W in the reaction $^{144}Sm(^{24}Mg, 7n)^{161}W$ with an alpha energy of 5.75 MeV. The corresponding peak was not resolved from the ^{157}Hf alpha peak, however. We observed here, Fig. 3, two well separated peaks with energies of 5,735 keV and 5,777 keV, which were assigned to ^{157}Hf and ^{161}W, respectively. This identification is based on a strong parent daughter correlation as demonstrated in Fig. 4. The half life obtained for the daughter ^{157}Hf is (110$\pm$6) ms in agreement with Ref. 21. The alpha branching ratio of (91 $\pm$7)% was calculated from the intensity ratio of the two alpha lines in the reaction $^{58}Ni+^{107}Ag \rightarrow ^{165}Re$ ($E^*=52$ MeV). The uncertainty of this ratio reflects a small possible direct production of ^{157}Hf in this reaction and the fact that the parent and daughter alpha lines are less well resolved in the position detector, Fig. 4. The half life of ^{161}W, measured with the chopper method, is (410$\pm$40) ms.

The isotope ^{153}Tm can be populated by alpha decay of ^{157}Hf with subsequent decay of ^{153}Yb, or by alpha decay of ^{157}Lu. The intensity balance for the various decay paths gives an alpha branching ratio of $\left(95^{+5}_{-8}\right)$% for ^{153}Tm which agrees well with the result of Hagberg et al. [2].

The identification of ^{161}Ta is particularly difficult because the corresponding alpha particle energy of (5,148$\pm$5) keV is the same within experimental uncertainties, as the energy of the ^{164}W alpha line. We base our identification on the following arguments: A strong peak at the above energy was seen both in the reaction $^{58}Ni+^{109}Ag \rightarrow ^{167}Re$ ($E^*=51$ MeV) and in the reaction $^{58}Ni+^{107}Ag \rightarrow ^{165}Re$ ($E^*=54$ MeV). In the former reactions copious production of ^{164}W via a $p2n$ reaction is expected from evaporation calculations. Simultaneous production of ^{161}Ta via an

$\alpha 2n$ mechanism cannot be excluded, although the velocity filter is partially selective for the $p2n$ channel. In the latter reaction, however, it is highly unlikely that a large cross section exists for the $1p$ channel leading to ^{164}W, since the compound nucleus excitation energy is as high as 54 MeV. On the other hand a large production of ^{161}Ta in this reaction via a $2p2n$ process is supported by evaporation calculations. This identification is further confirmed by the observation that the excitation function for ^{157}Lu was found to be consistent with its interpretation as daughter of the isotope assigned to the 5,148 keV peak.

3.3. Decay Chain of ^{163}Re (Fig. 6c)

Isotopes in this decay chain could be followed down to the known alpha decay of ^{155}Lu in the reactions ^{58}Ni + ^{107,109}Ag, Fig. 7. Time correlations between ^{155}Lu and a number of possible parent lines showed that a peak at (5,601 ± 6) keV is to be assigned to the alpha precursor ^{159}Ta. The half life of the daughter ^{155}Lu was found to be (70 ± 6) ms in agreement with the results of Macfarlane [21]. With the same method ^{163}Re was identified as precursor of ^{159}Ta. The alpha energy of ^{163}Re is (5,918 ± 6) keV. The half life of ^{159}Ta is (570 ± 180) ms from time correlations with ^{163}Re. The ^{163}Re half life of (260 ± 40) ms was measured with the chopper method. The alpha branching ratios of ^{155}Lu and ^{159}Ta were found to be (79 ± 4) % and (80 ± 5) %, respectively. A determination of the alpha branching ratio for ^{163}Re was not possible. An estimate gives a value of about 78 %.

The decay of ^{163}W is well known from previous experiments [19]. The corresponding alpha line at (5,384 ± 5) keV was observed here in reactions leading to Re and W compound nuclei, it was missing in reactions leading to Ta compound nuclei. The half life was determined by the chopper method. Its value of (3.0 ± 0.2) s agrees well with the value given by Eastham and Grant [19]. The measured alpha branching ratio of ^{163}W is (41 ± 5) %. It was determined from a comparison to the alpha peak intensities of ^{167}Os and ^{163}W in the reaction ^{84}Kr + ^{nat}Zr [5]. The isotope ^{159}Hf is populated mainly indirectly by alpha decay of ^{163}W and β decay of ^{159}Ta in the reaction ^{58}Ni + ^{109}Ag → ^{167}Re ($E^* = 51$ MeV). Direct production of ^{159}Hf via an $\alpha p3n$ reaction is highly unlikely at the indicated compound nucleus excitation energy and its observation behind the velocity filter partially suppressed. From the indirect feeding processes we obtain (12 ± 1) % for the alpha branching of ^{159}Hf. Similar arguments hold for the alpha branching of ^{155}Yb for which the value (84 ± 10) % was determined. The half life of ^{155}Yb, (1,590 ± 220) ms was measured by time correlation and agrees with published values [6, 22].

3.4. Decay Chain of ^{164}Re (Fig. 6d)

In this section the arguments leading to the assignment of new isotopes for some of the observed alpha lines are somewhat weaker than in the preceding sections. On the other hand the complete identification of all the new isotopes in the ^{163,162,161}Re chains of Figs. 6a, b, c excludes a large number of possible candidates for the alpha lines to be discussed here.

In the reaction ^{58}Ni + ^{109}Ag → ^{167}Re ($E^* = 51$ MeV) a weak alpha line was observed at (5,778 ± 10) keV, some 140 keV lower than the ^{163}Re alpha line, Fig. 7. The isotope ^{161}W, which emits an alpha particle with the same energy, could be excluded, because the ^{157}Hf daughter could not be seen. The ratio of the intensity of this new alpha line to the intensity of the ^{163}Re line decreased when the excitation energy of the compound nucleus was increased to 58 MeV. We assign the new line to ^{164}Re. The half life of (0.9 ± 0.7) s was determined with the chopper method. No correlations with daughter decays were measured.

A pair of peaks at (5,920 ± 10) keV and (5,878 ± 10) keV was found to have a parent daughter correlation

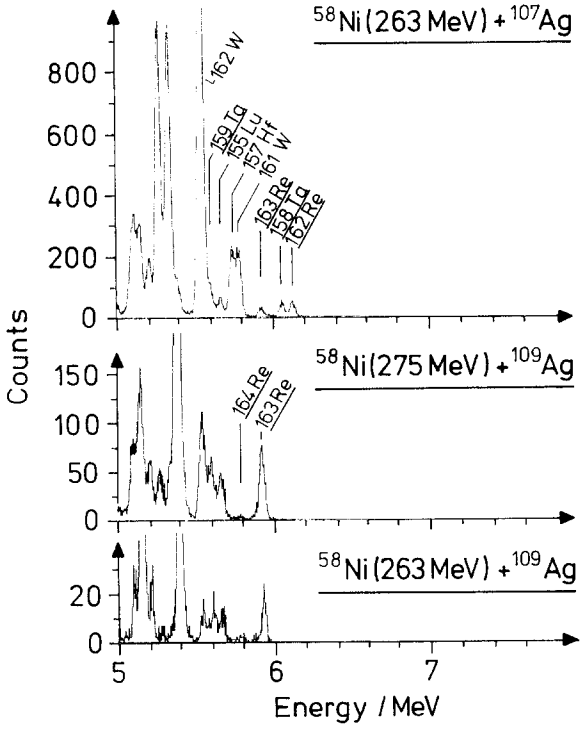

Fig. 7. High energy part of α singles spectra showing the α lines of the new isotopes ^{158,159}Ta and ^{162,163,164}Re

and was assigned to $^{160}W-^{156}Hf$. The identification of the element tungsten for the higher energy line followed unambiguously from cross bombardments. The mass was assigned by comparison of the excitation function behaviour to that of the previously identified pair $^{161}W-^{157}Hf$. The correlation method gave a half life of (25 ± 4) ms for ^{156}Hf and an alpha branching ratio of 100% (>81%).

3.5. Two New Alpha Unstable High Spin Isomers

Two short lived high energy transitions were observed in various reactions. A peak at $(7{,}408\pm10)$ keV was seen in reactions of ^{58}Ni projectiles with ^{107}Ag, ^{102}Pd, ^{103}Rh, ^{102}Ru, and ^{100}Ru targets, a peak at $(7{,}804\pm15)$ keV was seen with ^{107}Ag, ^{102}Pd, ^{103}Rh, and ^{102}Ru targets. Both lines are seen in Fig. 8. In this figure individual events observed during an irradiation of ^{103}Rh are plotted as function of time, the ordinate is the energy. For the two high energy lines one can clearly see the increase of the activity during the beampulse and the decay during the macro-pause. The time was synchronized with the macropulse period.

The half life of (2.7 ± 0.3) ms for the 7.41 MeV line was calculated by fitting an exponential decay function to the intensity during the beam pulses. A time correlation analysis between evaporation residue signals and alpha particle signals gave the half life (0.52 ± 0.16) ms for the 7.80 MeV line.

To our knowledge, alpha lines with the observed energies and half lives have not been reported in the literature. They do not fit into the systematics of ground state transitions and are very likely emitted from high spin isomers as will be discussed later. We could not find a correlation to any of the other alpha lines that we observed. A possible explanation is that the daughters are β emitters around $N=82$.

A number of cross bombardments have been done in an attempt to identify the high energy alpha emitters. A complete and unambiguous identification has not been possible as yet. Noting however, that the 7.41 MeV transition was observed in reactions leading to the compound nuclei ^{165}Re ($E^*=50$ MeV), ^{158}Hf ($E^*=60$ to 76 MeV) and was absent in fusion reactions leading to the compound nucleus ^{158}Yb at relatively high excitation energies ($E^*=78$ to 90 MeV), one can safely restrict the possible mass and charge range to $A=153$ to 156 and $Z=70$ to 72 with, perhaps, ^{154}Lu ($N=83$) being a best candidate. The second alpha emitter (7.80 MeV transition) is limited to a similar mass and charge range. Experiments to achieve full identification are in progress.

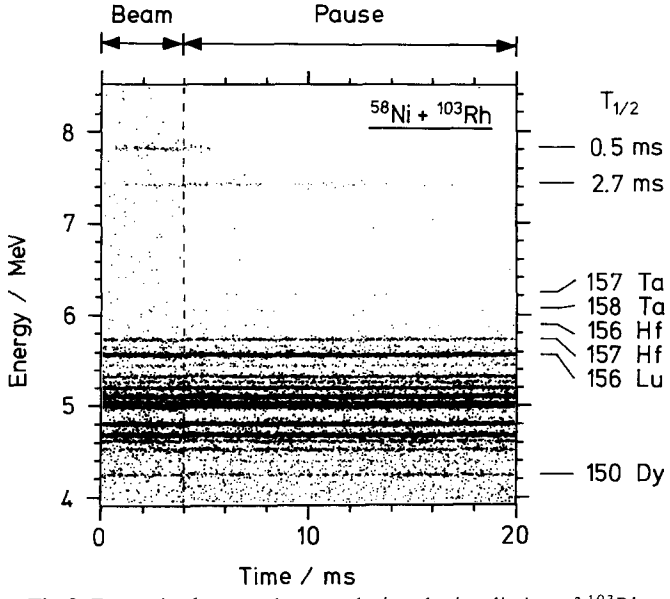

Fig. 8. Events in the stop detector during the irradiation of ^{103}Rh with ^{58}Ni ions of 276 MeV plotted in a two dimensional energy time coordinate system. This spectrum was measured synchronously to the 50 Hz macrostructure of the UNILAC beam. The two short living α lines of high energy show clearly a growth of their intensity during the irradiation and an exponential decay during the pulse pause. Further it should be pointed to the low background of scattered ^{58}Ni ions and evaporation residues during the beam pulse distributed over the whole energy region

4. Discussion

4.1. Q-Values and the Location of the Proton Drip Line

The data on the new alpha emitters identified in this work allow to broaden the Q_α systematics as is shown in Fig. 9. The alpha energies for the eleven new isotopes fit well into the general trend set by previously known alpha emitters. We have added data for the lightest known Osmium isotopes recently identified at Orsay [3], $^{165-168}Os$, and at our laboratory [5], $^{166-168}Os$. Close to the stability line these elements at and somewhat beyond the heavy end of the rare earths are generally considered to be transition nuclei. They have neutron numbers above 95, whereas the neutron numbers 84–90 involved here are just above the 82 closed neutron shell.

Since most of the isotopes investigated are very far from the stability line their α decay energies allow a stringent test of the various mass calculation schemes. A comparison of experimental and theoretical α energies is shown in Fig. 10 for the lightest known isotopes of Hf, Ta, W, and Re. The literature contains a large number of attempts to predict nuclear masses. We have confined ourselves here to a

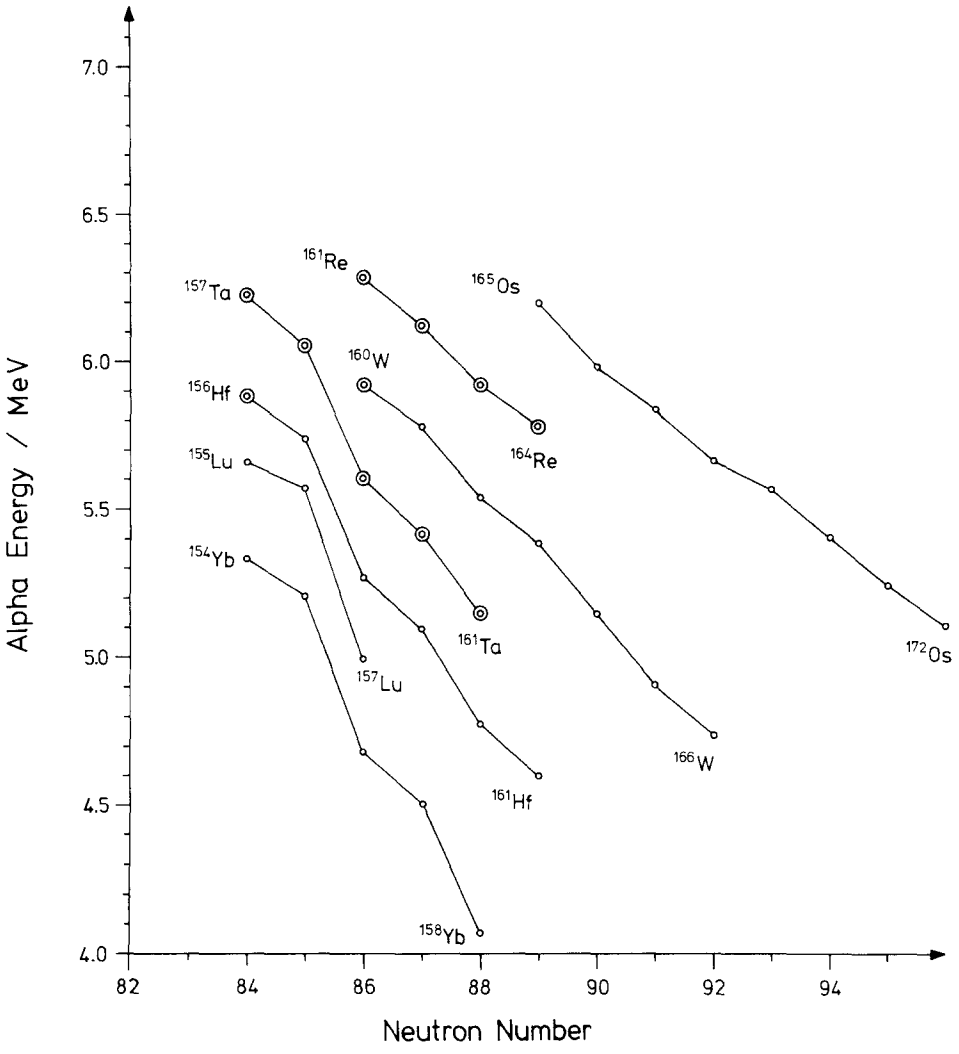

Fig. 9. Alpha systematics of neutron deficient isotopes of elements from Yb to Os. The new isotopes are marked with a second circle. They fit very well into the systematics of the previously known isotopes

comparison with five different approaches which are conveniently tabulated [24] and which can be assigned to three different philosophies. The first three approaches due to Myers, v. Groote-Hilf-Takahashi, and Seeger-Howard use the droplet model [25] to predict average trends and superpose various structural terms, essentially a pairing and a shell correction term. Myers and v. Groote-Hilf-Takahashi use relatively simple but different analytical expressions for the shell correction which are assumed to be damped as a function of nuclear deformation. The Seeger-Howard calculation includes shell corrections obtained explicitly with the Nilsson model and the Strutinski procedure. In contrast to the other mass estimates to be discussed later, the calculations based on the droplet model use also fission barriers in addition to known ground state masses to adjust the parameters of the theory.

As can be seen from Fig. 10 all the predictions based on the droplet model are very similar and reproduce the experimental data quite well. In particular, the values given by Myers agree generally within 200 keV with the data. Since the analytical shell correction term has an inherently smooth behaviour as a function of N and Z in-between shells, it is not surprising that small irregularities such as the somewhat larger drop in the experimental Q_α values from $N=85$ to $N=86$ for Hf and Ta, which has also been observed for Lu and Yb, Fig. 9, is not reproduced. A general trend seems to be that in this region the Q_α values are slightly overestimated by theory.

The predictions by Liran and Zeldes represent a shell approach to nuclear masses. Various mass regions limited by magic neutron and proton numbers are generally treated with different parameter sets. The nuclei of interest here are in a mass region where up

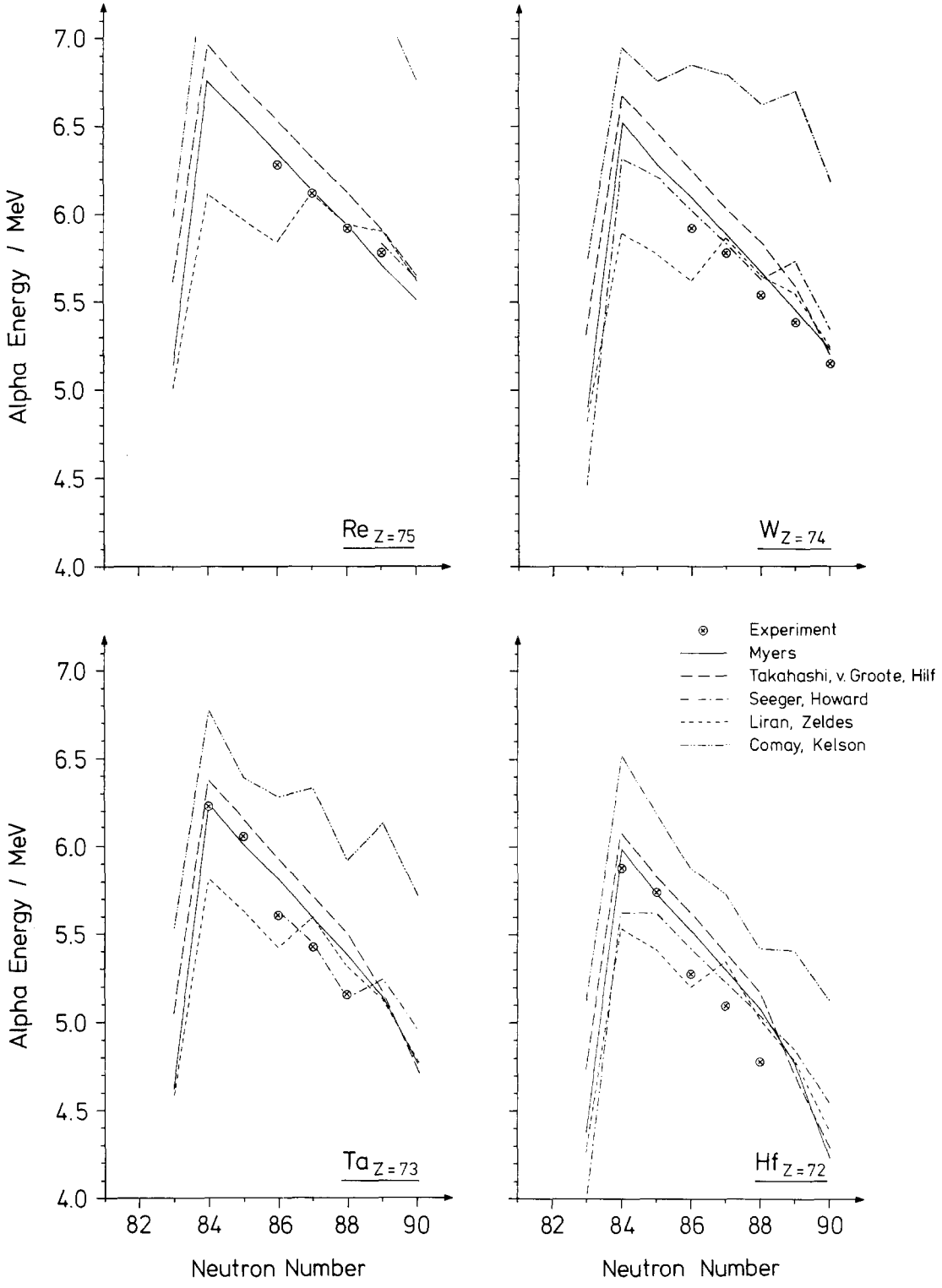

Fig. 10. Comparison of α energies of Re, W, Ta, and Hf isotopes near the closed neutron shell $N=82$ with predictions of five different mass tables [24]

to 32 parameters have been adjusted. Despite this very large number of adjustable parameters the predictions are generally of similar or even slightly less quality than those of the droplet model approaches and show fluctuations which are not present in the data.

The third philosophy for mass predictions is inspired by the Garvey-Kelson mass relations and is represented here by the table of Comay and Kelson who use the transverse Garvey-Kelson equation and average over many different subsets of experimentally known masses. This method claims to be parameter-free, but all sufficiently well known masses are used as input for the predictions.

As can be seen from Fig. 10 the predictions for Q_α values are rather poor in this mass region since errors exceed 1 MeV for the W and Re isotopes. We note that close to known masses this approach generally "fits" absolute masses typically within 100 keV.

An interesting problem arising with very proton rich nuclei is the location of the proton drip line and the possible occurance of proton radioactivity. In Fig. 11 we have plotted the proton binding energies predicted by Myers for Re and Ta as a function of neutron number. We note from Fig. 10 that the Q_α values calculated by Myers are in excellent agreement with our data for Re. It seems therefore justified to use these calculations to locate the proton drip line. As can be seen from Fig. 11 at least one, ^{161}Re, and possibly a second, ^{157}Ta, of the isotopes identified in this work, marked with circles in the Fig. 11, are proton unbound. In particular, ^{161}Re is predicted to be unbound by as much as 350 keV a value which seems to be in excess of the overall accuracy of the

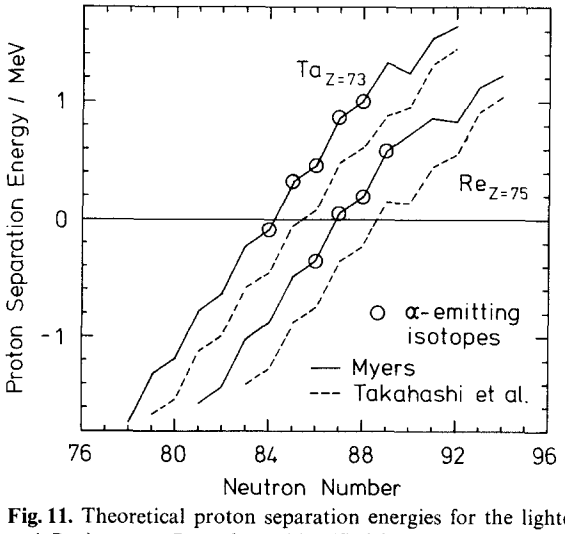

Fig. 11. Theoretical proton separation energies for the lightest Ta and Re isotopes. By α decay identified isotopes are marked by a circle

calculations of Myers in this mass region. We conclude that it is very likely that the proton drip line has been crossed experimentally for Re. However, evidence for a proton transition has not been seen in the low energy (<500 keV) part of our spectra. The search for proton radioactivity was beyond the scope of this work. Due to the general background from α decaying isotopes and from α particles leaving the stop detector in backward direction, only a strong proton branch could have been seen in the experimental arrangement used here. Estimates of proton half lives also show that for transition energies smaller than 400 keV in this mass region the proton branch is likely to be very small, as compared to the alpha branch. The systematics shown in Fig. 11 lead one to believe that ^{159}Re as well as ^{155}Ta are good candidates for proton radioactivity. For $N<84$ competition from alpha decay is expected to be weak. We note, see dashed line in Fig. 11, that v. Groote-Hilf-Takahashi predict lesser bound protons by about 250 keV in agreement with their trend to higher Q_α values, Fig. 10.

4.2. Alpha and Beta Decay Probabilities

In order to show the dependence of α decay probabilities on nuclear structure, we have drawn in Fig. 12 the reduced α widths, w_α, as function of proton number over a wide range from $Z=60$ to $Z=73$, separately for even and odd proton numbers, and separately for the neutron numbers $N=84$, 85, and 86.

The reduced α widths $w_\alpha \sim \lambda_\alpha/P$ were calculated with the barrier penetrabilities P and the partial α decay constant λ_α ($\lambda_\alpha = b_\alpha \cdot \ln 2/T_{1/2}$, b_α is the α branching ratio and $T_{1/2}$ is the total half life). The barrier penetrability was calculated with a WKB method [26]. As experimental input values we used the values given in Table 2 and for the elements Neodymium to Erbium the values given in Ref. 27 to Ref. 34. The errors were determined by the compounded uncertainties of the experimental branching ratios, half lives, and Q_α-values. All reduced widths were calculated assuming *s*-wave α particles and were normalized to the reduced width of the ^{212}Po ground state transition.

Reduced widths with the smallest experimental errors are available for the $N=84$ isotones, Fig. 12a. Theoretical calculations of Macfarlane et al. [35] for the $N=84$ isotones, with BCS wave functions and pure shell model wave functions show, in agreement with the experimental data, a dip of the α widths at the sub-shell $Z=64$. In filling the $\pi h_{11/2}$ sub-shell the calculated widths run through a mid-shell maximum at $Z=70$–72, whereas the experimental data show a

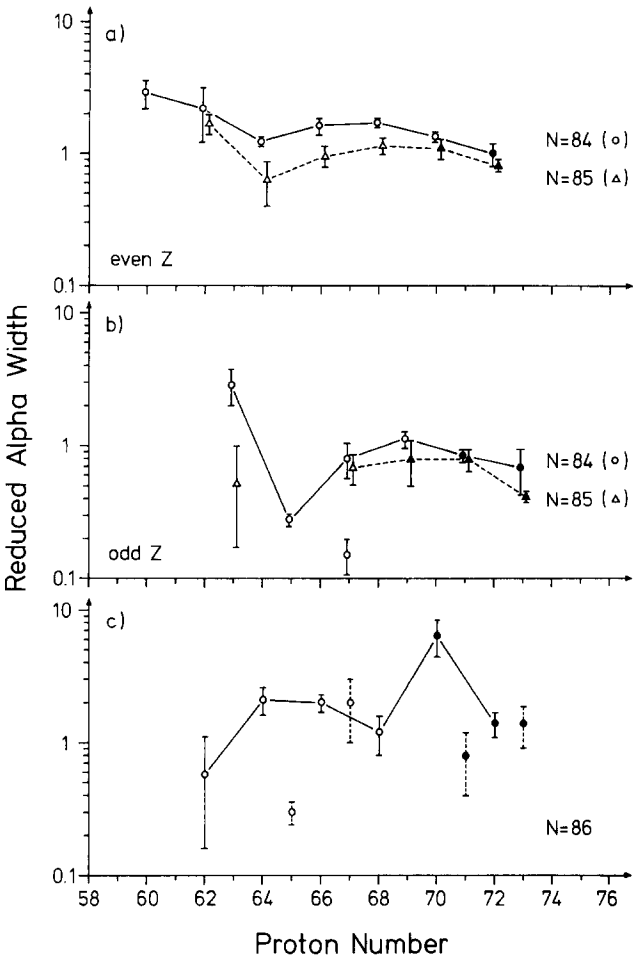

Fig. 12. Reduced α widths of $N=84$, 85, and 86 isotones as function of the proton number. For isotopes marked with filled symbols newly measured α branchings, half lives, or energies were used

maximum at $Z=68$. Possibly, the reason for the earlier decrease of the α widths are strong admixtures of the $\pi d_{3/2}$ shell. For this subshell relative small widths were calculated [35].

The dashed curve in Fig. 12a connects the widths of the odd $N=85$ isotones. These values show the same dependence as function of the proton number, but are in general 20% to 40% lower. This indicates that for the $N=85$ isotones s-wave α particle decay is most likely with configurations very similar to those involved in the even-even isotones, except for a moderate odd particle blocking effect [36].

The full line connecting the odd Z, $N=84$ isotones of Fig. 12b is, except for a shift of one unit on the proton number scale very similar to the dashed line, Fig. 12a. We conclude that the odd proton blocking effect on the α widths is similar in magnitude to the odd ($N=85$) neutron blocking. Finally, we note that the α widths of all odd-odd nuclei (dashed line, Fig. 12b) are on the average about 30% lower than the α widths of the odd-even and even-odd nuclei.

For the $N=86$ isotones considerable difficulties arise to determine exact α branchings because of the increasing competition from β decay. Therefore the reduced widths are known only with a relatively large error, Fig. 12c. Nevertheless, one can see that the reduced widths are on the average about 30% larger than the widths of the even-even $N=84$ isotones.

Assuming a reduced α width of one we have calculated partial α half lives which are compared with the experimental α half lives in columns 6 and 7 of Table 2. Predictions are given for the unknown α half lives and may be off by about 30%, corresponding to the variation of the reduced α widths.

Experimental and theoretical β half lives are compared in the two last columns of Table 2. The theoretical values are taken from calculations with the gross theory of β decay of Takahashi et al. [37]. The theoretical values, listed in Table 2, imply a Gaussian β strength function and allow for the occurrance of transitions to low lying states. They differ from the experimental values on the average by only 40%. Therefore, the theoretical β half lives were used together with the theoretical α half lives to calculate α branchings using the expression $b_\alpha = T_\beta/(T_\alpha + T_\beta)$. These values are presented in column 5 of Table 2.

4.3. High Spin Isomers

A complete discussion of the high energy transitions at 7.41 MeV and 7.80 MeV, observed here, has to be deferred until definite identification has been obtained. However, the measured energies and half lives allow us to estimate reduced alpha widths for these transitions assuming that the alpha branching ratio is 1. This is summarized in Table 3. One finds a rather

Table 3. Comparison of the half lives of the two high energetic α lines with calculations for different changes in angular momentum. The calculations for $\Delta l=0\hbar$ show the hindrance of α decay by a factor of about 10^5 in both cases

	E_α/keV	$T_{1/2,\mathrm{exp}}$	E_α/keV	$T_{1/2,\mathrm{exp.}}$
	7,408±10	(2.7±0.3) ms	7,804±15	(0.52±0.16) ms
$\Delta l_\alpha/\hbar$	W_α	$T_{1/2,\mathrm{theory}}$	W_α	$T_{1/2,\mathrm{theory}}$
0	$2\cdot10^{-5}$	60 ns	$1\cdot10^{-5}$	6 ns
8	0.02	50 μs	0.01	5 μs
10	0.6	1.7 ms	0.3	0.16 ms
12	380	100 ms	170	9 ms

strong hindrance of about 10^5 if one assumes s-wave alpha decay, an indication of a possible high spin isomerism. One obtains reduced widths closer to 1, again relative to the ^{212}Po ground state decay, if one assumes an angular momentum change of $(10\pm2)\hbar$ (Table 3).

Further we estimate, by comparison with the ground state Q_α values for the isotope region of interest (see Sect. 3.5), that the corresponding states are about 2 MeV to 3 MeV above ground state.

It is interesting to note in this context that a number of isomers in this energy range have been found for proton rich nuclei near the $N=82$ shell in reactions with α and ^{16}O beams. Broda et al. [38] report on a positive parity state in ^{147}Gd at 2.76 MeV with spin $21/2\hbar$. A 0.5 μs isomer was found by Daly et al. [39] in ^{148}Dy at 2.92 MeV with a spin of $10\hbar$. These isomers have been explained in terms of shell model configurations [38] in the vicinity of ^{146}Gd, which is interpreted as a doubly closed shell configuration [40]. Finally, we add that the approximate isotopic assignments given in Sect. 3.5 for the two high energy transitions are inside a region of isotopes where evidence for very high spin isomers has been found recently [7].

5. Outlook

Evaporation residues from fusion of ^{58}Ni ions and targets of Rh, Pd, and Ag have been studied. Due to the very low background after separation by the velocity separator SHIP and due to special detection methods extremely neutron deficient isotopes have been identified.

Until now only the α decay properties of these isotopes were investigated. Extensions of the experiments to α, γ and α, X-ray coincidences are planned. Information about the atomic number and about α transitions to excited nuclear states of the daughter nucleus is expected to be obtained.

With a detector telescope it should be possible to reduce the background in the spectra between 1 MeV and 2 MeV in order to observe proton radioactivity.

By increasing the excitation energy further new isotopes with production cross sections down to values in the region of nb may be detected. These experiments will show the limitations set to the production of new neutron deficient isotopes by heavy ion reactions below the closed proton shell $Z=82$.

The authors acknowledge with pleasure the help of many groups which supported our experiments. Especially we thank the accelerator group providing excellent beams and the target laboratory producing our targets. Data collection and data analysis have become possible by the achievements provided by the experimental electronics group and the program development group of the GSI computer center.

References

1. Mang, H.J.: Ann. Rev. Nucl. Sci. **14**, 1 (1964)
2. Hagberg, E., Hansen, P.G., Hardy, J.C., Hornshøj, P., Jonson, B., Mattsson, S., Tidemand-Petersson, P.: Nucl. Phys. A**293**, 1 (1977)
3. Cabot, C., Della Negra, S., Deprun, C., Gauvin, H., Le Beyec, Y.: Z. Physik A**287**, 71 (1978)
4. Schmidt-Ott, W.-D., Schrewe, U.J., v. Dincklage, R.-D., Hiller, W.J.: GSI Jahresbericht 1977, GSI-J-1-78, 81 (1978)
5. Faust, W., Hofmann, S., Münzenberg, G., Reisdorf, W., Valli, K., Ewald, H., Güttner, K.: GSI Jahresbericht 1976, GSI-J-1-77, 81 (1977)
6. Gauvin, H., Le Beyec, Y., Livet, J., Reyss, J.L.: Ann. Phys. **9**, 241 (1975)
7. Pedersen, J., Back, B.B., Bernthal, F.M., Bjørnholm, S., Borggren, J., Christensen, O., Folkmann, F., Herskind, B., Khoo, T.L., Neiman, M., Pühlhofer, F., Sletten, G.: Phys. Rev. Lett. **39**, 990 (1977)
8. Ravn, H.L.: Proc. 3rd Int. Conf. on nuclei far from stability, Cargèse, CERN 76-13, 22 (1976)
9. Münzenberg, G., Faust, W., Hofmann, S., Armbruster, P., Güttner, K., Ewald, H.: to be published
10. Hofmann, S., Armbruster, P., Faust, W., Münzenberg, G., Reisdorf, W., Güttner, K.: GSI Jahresbericht 1977, GSI-J-1-78, 80 (1978)
11. Hofmann, S., Armbruster, P., Faust, W., Münzenberg, G., Schött, H.-J., Güttner, K.: GSI Jahresbericht 1977, GSI-J-1-78, 189 (1978)
12. Faust, W.: Das Geschwindigkeitsfilter SHIP – Beschreibung, Ausmessung, Berechnung des Wirkungsgrades und erste Experimente, Thesis, GSI-P-4-78 (1978)
13. Northcliffe, L.C., Schilling, R.F.: Nuclear Data Tables A**7**, 233 (1970)
14. Harmatz, B.: Nuclear Data Sheets **19**, 33 (1976)
15. Bowman, J.D., Hyde, E.K., Eppley, R.E.: Lawrence Berkeley Laboratory, Nuclear Chemistry Annual Report No. LBL-1666 p. 4 (1972)
16. Toth, K.S., Bingham, C.R., Schmidt-Ott, W.-D.: Phys. Rev. C**10**, 2550 (1974)
17. Schmidt-Ott, W.-D., Toth, K.S., Newman, E., Bingham, C.R.: Phys. Rev. C**10**, 296 (1974)
18. Toth, K.S., Hahn, R.L., Bingham, C.R., Ijaz, M.A., Walker, R.F.: Phys. Rev. C**7**, 2010 (1973)
19. Eastham, D.A., Grant, I.S.: Nucl. Phys. A**208**, 119 (1973)
20. Toth, K.S., Schmidt-Ott, W.-D., Bingham, C.R., Ijaz, M.A.: Phys. Rev. C**12**, 533 (1975)
21. Macfarlane, R.D.: Phys. Rev. **137**, 1448 (1964)
22. Macfarlane, R.D.: Phys. Rev. **136**, 941 (1964)
23. Macfarlane, R.D., Griffioen, R.G.: Phys. Rev. **131**, 2176 (1963)
24. Maripuu, S. (ed.): 1975 Mass Predictions, Atomic Data and Nuclear Data Tables **17**, Nos. 5–6, 476 (1976)
25. Myers, W.D., Swiatecki, W.J.: Ann. Phys. **55**, 395 (1969)
26. Rasmussen, J.O.: Phys. Rev. **113**, 1593 (1959)
27. Burrows, T.W.: Nucl. Data Sheets **12**, 203 (1974)
28. Burrows, T.W.: Nucl. Data Sheets **14**, 413 (1975)
29. Burrows, T.W., Auble, R.L.: Nucl. Data Sheets **16**, 231 (1975)
30. Baglin, C.M.: Nucl. Data Sheets **18**, 223 (1976)
31. Harmatz, B.: Nucl. Data Sheets **19**, 33 (1976)
32. Holland, G.E.: Nucl. Data Sheets **19**, 337 (1976)

33. Harmatz, B., Shepard, J.R.: Nucl. Data Sheets **20**, 373 (1977)
34. Harmatz, B., Ewbank, W.B.: Nucl. Data Sheets **25**, 113 (1978)
35. Macfarlane, R.D., Rasmussen, J.O., Rho, M.: Phys. Rev. **134**, 1196 (1964)
36. Mang, H.J.: Ann. Rev. Nucl. Science **14**, 1 (1964)
37. Takahashi, K., Yamada, M., Kondoh, T.: Atomic Data and Nucl. Data Tables **12**, 101 (1973)
38. Broda, R., Ogawa, M., Lunardi, S., Maier, M.R., Daly, P.J., Kleinheinz, P.: Z. Physik A**285**, 423 (1978)
39. Daly, P.J., Kleinheinz, P., Broda, R., Stefanini, A.M., Lunardi, S., Backe, H., Richter, L., Willwater, R., Weik, F.: Z. Physik A**288**, 103 (1978)
40. Kleinheinz, P., Ogawa, M., Broda, R., Daly, P.J., Haenni, D., Beuscher, H., Kleinrahm, A.: Z. Physik A**286**, 27 (1978)
41. Takahashi, K., v. Groote, H., Hilf, E.R.: Gross Theory of Nuclear Masses and Radii, IKDA 76/26, Institut für Kernphysik, Technische Hochschule Darmstadt (1976)

S. Hofmann
W. Faust
G. Münzenberg
W. Reisdorf
P. Armbruster
Gesellschaft für Schwerionenforschung mbH
Postfach 110541
D-6100 Darmstadt 11
Federal Republic of Germany

K. Güttner
H. Ewald
II. Physikalisches Institut
Justus Liebig-Universität
D-6300 Gießen
Federal Republic of Germany